J. Fluid Mech. (1984), *vol.* 140, *pp.* 373–395
Printed in Great Britain

The effects of curvature on the flow field in rapidly rotating gas centrifuges

By HOUSTON G. WOOD,
University of Virginia, Charlottesville, Virginia

JO ANN JORDAN
Union Carbide Corporation, Nuclear Division, Oak Ridge, Tennessee

AND MAX D. GUNZBURGER
Carnegie–Mellon University, Pittsburgh, Pennsylvania

(Received 15 August 1983 and in revised form 7 November 1983)

The effects of curvature on the fluid dynamics of rapidly rotating gas centrifuges are studied. A governing system of a linear partial differential equation and boundary conditions is derived based on a linearization of the equations for viscous compressible flow. This system reduces to the Onsager pancake model if the effects of curvature are neglected. Approximations to the solutions of the governing equations with and without curvature terms are obtained via a finite-element method. Two examples are considered: first where the flow is driven by a thermal gradient at the wall of the centrifuge, and then for the flow being driven by the introduction and removal of mass through the ends of the centrifuge. Comparisons of the results obtained show that, especially for the second example, the inclusion of the terms due to curvature in the model can have an appreciable effect on the solution.

1. Introduction

Over the past few years, increasing interest has been shown in determining the flow inside a gas centrifuge. This interest is mostly due to the facts that centrifugation has become a viable, energy-efficient method for enriching uranium in its fissionable isotope and that the separative efficiency of a gas centrifuge is determined largely by the dynamics of the fluid flow within the centrifuge (Von Halle 1977; Hoglund, Shacter & Von Halle 1979). One of the most popular models for describing this internal flow consists of the *Onsager 'pancake' equation* and the *Carrier–Maslen boundary conditions*. For a full derivation and discussion of this formulation see Wood & Morton (1980) and Babarsky & Wood (1982). These equations have been approximately solved by a variety of techniques, including eigenfunction-expansion methods (Wood & Morton 1980); finite-difference methods (Viecelli 1983); and finite-element methods (Gunzburger & Wood 1982; Gunzburger, Wood and Jordan 1983).

The two main assumptions invoked in deriving the Onsager equation are that the flow field is a small perturbation about an isothermal solid-body rotation and that the rotational speed of the centrifuge is high enough so that the bulk of the fluid is found in the region adjacent to the outer wall of the centrifuge. Mathematically, the first assumption enables one to linearize the governing equations, i.e. the equations of viscous compressible flow, while the second assumption allows for the neglect of

terms that are due to the curvature of the outer wall of the centrifuge. The utility of these assumptions in simplifying the mathematical description of the flow field is obvious. Linear equations are generally easier to solve than nonlinear ones, and neglecting the effects of curvature also greatly simplifies the governing system. The ability to approximate the solution of the model equations by eigenfunction-expansion methods is greatly facilitated by these simplifications. Recently, Jung (1983) has reported attempts to construct sets of expansion functions while retaining curvature terms in the model equations.

Assumptions such as those described above are usually justified *a priori* by observations or intuition. *A posteriori*, they are justified by comparisons of data obtained through the use of these assumptions with experimental data and/or data obtained from more complicated models which do not involve the assumptions. It is the latter type of comparison, in the context of the curvature effects, which is of interest to us here. Specifically, we wish to explore the differences between solutions obtained with and without neglecting the effects of curvature. Fortunately, this comparison can be greatly facilitated by the use of purely numerical techniques. In fact, as is described in this paper, finite-element approximations which include the effects of curvature may be obtained just as easily as when curvature effects are neglected.

The plan of the remainder of the paper is as follows. In §2 we present a detailed derivation of the linear governing equations in which curvature terms have been retained. The presentation here is based on that of Maslen (1979). In §3 we discuss the numerical techniques employed in the approximation of the solution of the model equations derived in §2. Comparisons of solution with and without curvature effects are presented in §4, and some concluding remarks are made in §5.

2. The Onsager–Maslen model

2.1. *The Onsager–Maslen equation*

We assume that the centrifuge is a right circular cylinder of radius a and length L. Let (r, θ, z) be cylindrical coordinates with the origin fixed at the bottom of the cylinder and on the axis of rotation, and with the z-axis aligned along that axis. If the centrifuge rotates at an angular velocity Ω then

$$\left.\begin{aligned} &u = 0, \quad v = \Omega r, \quad w = 0, \\ &p = p_{\mathrm{w}} \exp\left\{-A^2\left[1-\left(\frac{r}{a}\right)^2\right]\right\}, \\ &T = T_0 = \text{constant}, \quad \rho = \frac{p}{RT_0} \end{aligned}\right\} \tag{2.1}$$

constitute a solution of the equations of compressible viscous flow corresponding to an isothermal solid-body motion of the fluid. In (2.1), (u, v, w) denote respectively the (r, θ, z)-components of velocity, p the pressure, ρ the density, T the temperature, R the specific gas constant, T_0 the uniform gas temperature, p_{w} the pressure at the wall of the cylinder, and $A = a\Omega/(2RT_0)^{\frac{1}{2}}$.

We will make five assumptions concerning the flow in the centrifuge. These are:

(i) the flow is steady;

(ii) the flow is axially symmetric;

(iii) the flow is a small perturbation from the isothermal solid-body rotation described in (2.1);

(iv) outside of the Ekman layers adjacent to the ends of the cylinder, the effects of axial diffusion may be neglected;

(v) the effects of radial diffusion of radial momentum may be neglected.

For a detailed discussion of these assumptions see Wood & Morton (1980).

Using these assumptions, the equations of conservation of mass, momentum and energy and the equation of state reduce to (Wood & Morton 1980; Babarsky & Wood 1982)

$$(r\rho u')_r + r\rho w'_z = 0, \tag{2.2}$$

$$2\Omega\rho v' + r\Omega^2\rho' = p'_r, \tag{2.3}$$

$$\mu(r^2 v'_r - rv')_r = 2\Omega r^2 \rho u', \tag{2.4}$$

$$\mu(rw'_r)_r = rp'_z, \tag{2.5}$$

$$k(rT'_r)_r = -\Omega^2 r^2 \rho u', \tag{2.6}$$

$$p' = \rho RT' + \rho' RT_0. \tag{2.7}$$

In (2.2)–(2.7), (u', v', w') denote the (r, θ, z)-components of the perturbed velocity field and ρ', p', T' are the perturbed density, pressure and temperature respectively. In the derivation of (2.2)–(2.7), we have also assumed that the viscosity μ and thermal conductivity k are functions of temperature only, and that the bulk viscosity vanishes. Furthermore, we have assumed that there are no sources of mass, momentum and energy present in the flow field.

Eliminating u' between (2.4) and (2.6) yields

$$\Omega\mu(r^2 v'_r - rv')_r = -2k(rT'_r)_r. \tag{2.8}$$

We may also eliminate the pressure between (2.3) and (2.5) to yield

$$\Omega^2 r\phi_z = -\mu\left[\frac{(rw'_r)_r}{\rho r}\right]_r, \tag{2.9}$$

where we have also used (2.7) and introduced the auxiliary variable

$$\phi = \frac{T'}{T_0} - \frac{2v'}{\Omega r}. \tag{2.10}$$

Integrating (2.8) and setting the integration constants to zero to satisfy boundedness conditions at the axis $r = 0$ yields

$$\Omega\mu(r^2 v'_r - rv') = -2k(rT'_r). \tag{2.11}$$

Using (2.6), (2.8), (2.10) and (2.11), we may then show that

$$\mu\left(\frac{r^3}{1+S(r/a)^2}\phi_r\right)_r = -4\rho r^2 u', \tag{2.12}$$

where $S = \mu\Omega^2 a^2/4kT_0$.

Equations (2.2), (2.9) and (2.12) form a system of three equations for u', w' and ϕ. We rewrite these equations in dimensionless form by letting $\eta = r/a$, $y = z/a$, $u = u'/\Omega a$, $w = w'/\Omega a$, $v = v'/\Omega r$, $\rho = \rho'/\rho_w$, $p = p'/p_w$ and $T = T'/T_0$, where $\rho_w = p_w/RT_0$ is the density at the vertical wall of the cylinder of the flow described by (2.1). In terms of these dimensionless variables, (2.2), (2.9) and (2.12) are respectively given by

$$(\eta\rho_0 u)_\eta + \eta\rho_0 w_y = 0, \tag{2.13}$$

$$Re\,\eta\phi_y = \left[\frac{(\eta w_\eta)_\eta}{\eta\rho_0}\right]_\eta \tag{2.14}$$

and

$$\left(\frac{\eta^3}{1+S\eta^2}\phi_\eta\right)_\eta = -4\,Re\,\rho_0\,\eta^2 u, \tag{2.15}$$

where $Re = \rho_w \Omega a^2/\mu$ is the Reynolds number, ϕ is now defined by

$$\phi = T - 2v, \tag{2.16}$$

and

$$\rho_0 = \frac{\rho}{\rho_w} = \exp\{-A^2(1-\eta^2)\} \tag{2.17}$$

is the dimensionless density of the flow described by (2.1). We now introduce the radial variable $x = A^2(1-\eta^2)$, which measures the distance from the wall of the cylinder in 'scale heights', i.e. e-folding heights of the ambient density, which by (2.17) is now given by $\rho_0 = \exp(-x)$. The system of equations (2.13)–(2.15) is now transformed to

$$-2A^2(\eta\,e^{-x}u)_x + e^{-x}w_y = 0, \tag{2.18}$$

$$Re\,\phi_y = 8A^6[e^x(\eta^2 w_x)_x]_x \tag{2.19}$$

and

$$A^4\left(\frac{\eta^4}{1+S\eta^2}\phi_x\right)_x = -Re\,\eta\,e^{-x}u, \tag{2.20}$$

where

$$\eta = \left[1-\frac{x}{A^2}\right]^{\frac{1}{2}}. \tag{2.21}$$

Our next goal is to reduce this system of equations to a single partial differential equation. The first step in this reduction is to define the stream function ψ by the relations

$$\psi_y = -\eta\,e^{-x}u \tag{2.22}$$

and

$$2A^2\psi_x = -e^{-x}w, \tag{2.23}$$

so that (2.18) is identically satisfied. Substituting (2.22) and (2.23) into (2.19) and (2.20) yields

$$Re\,\phi_y = -16A^8(e^x(\eta^2(e^x\psi_x)_x)_x)_x \tag{2.24}$$

and

$$A^4\left(\frac{\eta^4}{1+S\eta^2}\phi_x\right)_x = Re\,\psi_y. \tag{2.25}$$

Eliminating ϕ from these last two equations then yields

$$16A^{12}\left(\frac{\eta^4}{1+S\eta^2}(e^x(\eta^2(e^x\psi_x)_x)_x)_{xx}\right)_x + (Re)^2\psi_{yy} = 0. \tag{2.26}$$

We introduce the Onsager 'master potential' χ defined by

$$\psi = -2A^2\chi_x. \tag{2.27}$$

Substituting (2.27) into (2.26) yields

$$16A^{12}\left(\frac{\eta^4}{1+S\eta^2}(e^x(\eta^2(e^x\chi_{xx})_x)_x)_{xx}\right)_x + (Re)^2\chi_{xyy} = 0. \tag{2.28}$$

Integrating this last equation with respect to x and assuming that χ and all its derivatives are negligible for large x, we have that

$$(e^x(\eta^2(e^x\chi_{xx})_x)_x)_{xx} + \frac{B^2(1+S\eta^2)}{\eta^4}\chi_{yy} = 0, \tag{2.29}$$

where $B = Re/4A^6$. Equation (2.29) is the Onsager–Maslen equation. If we set $\eta = 1$ wherever it appears algebraically in (2.29) we obtain the Onsager 'pancake' equation (Wood & Morton 1980; Babarsky & Wood 1982). Thus the effects of curvature are included through the explicit appearance of η in the coefficients of the partial differential equation (2.29).

The differential equation (2.29) holds in the interior of the centrifuge except near the ends of the cylinder $y = 0$ and $y = L/a$ and at 'large' distances from the wall of the cylinder $x = 0$. In narrow Ekman layers near the ends of the cylinder, axial-diffusion effects become important, and the assumption through which this effect was neglected is no longer justified. At large distances from the wall of the centrifuge the gas becomes rarefied and the equations of motion, from which (2.29) was derived, no longer adequately model the flow field. These observations are considered in greater detail in §§2.2 and 2.3, where we derive the boundary condition that the master potential χ must satisfy.

2.2. *Radial boundary conditions*

We now examine the boundary conditions that the master potential χ must satisfy at the wall of the cylinder $x = 0$ and at the 'top of the atmosphere' $x = x_T$, where x_T is a distance in scale heights at which the gas becomes rarefied. In actual computations, the value of x_T is chosen by performing a series of calculations with different values of x_T, and then observing at what value of x_T the solutions, as functions of x_T, cease to appreciably change. If this fails to occur, as in cases of low rotation speeds, then x_T is set equal to the value of x at the axis, i.e. $x_T = A^2$.

At $x = x_T$ we assume that $u = v_x = w_x = T_x = 0$ (Wood & Morton 1980). Equations (2.24), (2.28) and the condition $w_x = 0$ easily yield

$$(e^x \chi_{xx})_x = 0 \quad \text{at} \quad x = x_T. \tag{2.30}$$

Equation (2.23) and the condition $u = 0$ yield $\psi_y = 0$ at $x = x_T$, or $\psi(x_T, y) = 0$, where the integration constant has been set to zero by setting the stream function to zero at $x = x_T$. Then, from (2.27),

$$\chi_x = 0 \quad \text{at} \quad x = x_T. \tag{2.31}$$

Equations (2.25), (2.28) and (2.29) combine into

$$Re\,\eta^4 \phi_{yx} = -32A^{10}B^2(1 + S\eta^2)\,\chi_{yy}.$$

Integrating with respect to y results in

$$Re\,\eta^4[\phi_x(x,y) - \phi_x(x,0)] = -32A^{10}B^2[1 + S\eta^2][\chi_y(x,y) - \chi_y(x,0)]. \tag{2.32}$$

But (2.16) and the condition $v_x = T_x = 0$ imply that $\phi_x(x_T, y) = 0$. Therefore evaluating (2.32) at $x = x_T$ yields that $\chi_y(x_T, y) = k_1$ for some constant k_1. Again integrating with respect to y, we have that $\chi(x_T, y) = k_1 y + k_2$ for some constants k_1 and k_2. Without loss of generality we may set $k_2 = 0$ because all variables of interest depend on derivatives of the master potential. We may also take $k_2 = 0$ since all variables of interest except ϕ_x depend on x-derivatives of χ, and by (2.32) ϕ_x depends on the difference $\chi_y(x,y) - \chi_y(x,0)$, which is again independent of k_1. (See §2.4 for a listing of the explicit dependence of physically interesting variables on the master potential χ.) With $k_1 = k_2 = 0$, we then have

$$\chi = 0 \quad \text{at} \quad x = x_T. \tag{2.33}$$

At the wall of the cylinder $x = 0$, we assume that the velocity perturbation vanishes, i.e. $u = v = w = 0$, and that the temperature T is prescribed, i.e. $T(0, y) = \theta(y)$. Equations (2.24) and (2.28) and the condition $w = 0$ yield

$$\chi_{xx} = 0 \quad \text{at} \quad x = 0. \tag{2.34}$$

Equations (2.23) and the condition $u = 0$ yield $\psi_y(0, y) = 0$. Integrating with respect to y yields $\psi(0, y) = k_3$ for some constant k_3. Since we have set the stream function equal to zero, k_3 represents the net mass flow through the bottom end of the cylinder. For simplicity we assume that $k_3 = 0$, and thus we will be restricted to problems that have no net mass flow through the bottom of the cylinder. Then $\psi(0, y) = 0$, or, using (2.28),

$$\chi_x = 0 \quad \text{at} \quad x = 0. \tag{2.35}$$

Equations (2.25) and (2.28) yield

$$Re\,\phi_y = 32A^{10}(e^x(\eta^2(e^x\chi_{xx})_x)_x)_x, \tag{2.36}$$

and (2.16) and the conditions $v = 0$ and $T_y = \theta_y(y)$ yield that $\phi_y(0, y) = \theta(y)$. Then evaluating (2.36) at $x = 0$ yields

$$(e^x(\eta^2(e^x\chi_{xx})_x)_x)_x = f(y) = \frac{Re}{32A^{10}}\theta_y(y) \quad \text{at} \quad x = 0, \tag{2.37}$$

where $\theta(y)$ is the prescribed dimensionless temperature along the wall.

Equation (2.30), (2.31), (2.33)–(2.35) and (2.37) are the six boundary conditions which the master potential χ must satisfy at the two fixed radial positions $x = 0$ and $x = x_T$. That there are six such boundary conditions needed is to be expected because equation (2.29) is a sixth-order differential equation with respect to x.

2.3. *The Carrier–Maslen boundary conditions*

To complete the specification of the problem, we need to determine the boundary conditions at the top and bottom of the cylinder. Since, in the derivation of (2.29), we have neglected all axial-diffusion terms, that equation does not adequately describe the flow in the Ekman layers adjacent to the top and bottom of the cylinder. Thus we view (2.29) as the governing equation outside the Ekman layers, and the task at hand is to derive equations that model the flow in the Ekman layers. The derivation below again follows that of Maslen (1979).

The starting point is, again, the equations of steady viscous compressible flow. We linearize these equations about the solid-body rotation described by (2.1). Subsequently, we apply standard techniques of boundary-layer analysis to conclude that Ekman layers have a thickness of order $1/(Re)^{\frac{1}{2}}$ and to derive a system of equations which hold in the Ekman layers. In terms of the dimensionless variables, these equations are given by (2.18),

$$\eta\,Re\,(2\,e^{-x}\tilde{v} + \tilde{\rho} + \tilde{p}_x) = -\tilde{u}_{yy}, \tag{2.38}$$

$$2\,Re\,e^{-x}\tilde{u} = \eta\tilde{v}_{yy}, \tag{2.39}$$

$$\tilde{p}_y = 0, \tag{2.40}$$

$$4\,Re\,S\eta\,e^{-x}\tilde{u} + \tilde{T}_{yy} = 0, \tag{2.41}$$

and

$$\tilde{p} = e^{-x}\tilde{T} + \tilde{\rho}, \tag{2.42}$$

where η is given by (2.22), and where $\tilde{}$ denotes a flow variable in the Ekman layer. Equation (2.16), (2.39) and (2.41) may be combined to yield

$$\eta\tilde{\phi}_{yy} = -4\,Re\,e^{-x}\tilde{u}(1 + S\eta^2). \tag{2.43}$$

Equations (2.16), (2.38), (2.40) and (2.42) may be combined to yield

$$\eta\, Re\, e^{-x}\tilde{\phi}_y = \tilde{u}_{yyy}. \tag{2.44}$$

Let us focus for the moment on the vicinity of the bottom of the cylinder, i.e. $y = 0$. The solution of (2.43) and (2.44), which remains bounded as y increases, is readily found to be

$$\tilde{u} = A(x)f_1(y) + B(x)f_2(y) \tag{2.45}$$

and

$$\frac{\eta[\tilde{\phi} - C(x)]}{2[1+S\eta^2]^{\frac{1}{2}}} = \mathrm{i}A(x)f_1(y) - \mathrm{i}B(x)f_2(y), \tag{2.46}$$

where $A(x)$, $B(x)$ and $C(x)$ are arbitrary functions, $\mathrm{i} = (-1)^{\frac{1}{2}}$,

$$f_1(y) = \exp[-(\mathrm{i}\beta)^{\frac{1}{2}}y], \quad f_2(y) = \exp[-(-\mathrm{i}\beta)^{\frac{1}{2}}y] \tag{2.47}$$

and

$$\beta = 2\, Re\, e^{-x}(1+S\eta^2)^{\frac{1}{2}}. \tag{2.48}$$

Also, using (2.23) and (2.45), we may deduce that

$$\frac{(2\beta)^{\frac{1}{2}}[(\tilde{\psi} - D(x)]}{\eta\, e^{-x}} = (1-\mathrm{i})\,A(x)f_1(y) + (1+\mathrm{i})\,B(x)f_2(y), \tag{2.49}$$

where $D(x)$ is again an arbitrary function. As $(Re)^{\frac{1}{2}}y \to \infty$, the Ekman variables $\tilde{\phi}(x,y)$ and $\tilde{\psi}(x,y)$ must match the values of the corresponding outer variables $\phi(x,y)$ and $\psi(x,y)$ as $y \to 0$. Then, from (2.46) and (2.47) we have that $C(x) = \phi(x,0)$ and $D(x) = \psi(x,0)$ respectively. Now, by (2.47), $f_1(0) = f_2(0) = 1$, so that, if we evaluate (2.45)–(2.47) at $y = 0$, we have that

$$\overline{u^-}(x) = A(x) + B(x),$$

$$\frac{\eta[\overline{\phi^-}(x) - \phi(x,0)]}{2[1+S\eta^2]^{\frac{1}{2}}} = \mathrm{i}A(x) - \mathrm{i}B(x)$$

and

$$\frac{(2\beta)^{\frac{1}{2}}[\overline{\psi^-}(x) - \psi(x,0)]}{\eta\, e^{-x}} = (1-\mathrm{i})\,A(x) + (1+\mathrm{i})\,B(x),$$

where $\overline{(\,)^-}$ denotes a prescribed value at the bottom end of the cylinder. The functions $A(x)$ and $B(x)$ may be easily eliminated from these last three equations to yield, with the help of (2.48),

$$4\eta^{-2}[Re\, e^x]^{\frac{1}{2}}[1+S\eta^2]^{\frac{3}{4}}(\psi(x,0) - \overline{\psi^-}(x)] + 2\eta^{-1}[1+S\eta^2]^{\frac{1}{2}}\overline{u^-} + \phi(x,0) - \overline{\phi^-}(x) = 0. \tag{2.50}$$

Similarly, we may derive the analogue of (2.50) that is valid at the top of the cylinder $y = y_T = L/a$. If $\overline{(\,)}$ denotes a prescribed value at the top of the cylinder, this relation is given by

$$4\eta^{-2}[Re\, e^x]^{\frac{1}{2}}[1+S\eta^2]^{\frac{3}{4}}(\psi(x,y_T) - \overline{\psi}(x)] + 2\eta^{-1}[1+S\eta^2]^{\frac{1}{2}}\bar{u}(x) + \phi(x,y_T) - \overline{\phi}(x) = 0. \tag{2.51}$$

Equations (2.50) and (2.51), which are known as the Carrier–Maslen boundary conditions, relate the interior variables ψ and ϕ to the prescribed boundary conditions at the ends of the cylinder. Our remaining task is to recast (2.50) and (2.51) in terms of the master potential χ defined by (2.28).

Equations (2.26) and (2.28) may be combined to yield

$$A^2\left(\frac{\eta^4}{1+S\eta^2}\phi_x\right)_x = -Re\,\chi_{xy}.$$

Integrating with respect to x and using the radial boundary conditions $\phi_x(x_T, y) = 0$ and $\chi_y(x_T, y) = 0$ (see §2.2) then yields

$$\phi_x = -\frac{2\,Re}{A^2\eta^4}(1+S\eta^2)\,\chi_y. \tag{2.52}$$

Differentiating (2.50) with respect to x and then using (2.52) evaluated at $y = 0$ to eliminate $\phi_x(x, 0)$, and (2.28), also evaluated at $y = 0$, to eliminate $\psi(x, 0)$ yields

$$B^2\eta^{-4}[1+S\eta^2]\,\chi_y(x,0)+2AB^{\frac{3}{2}}\{\eta^{-2}[1+S\eta^2]^{\frac{3}{4}}\,e^{\frac{1}{2}x}\,\chi_x(x,0)\}_x$$
$$= g^-(x) = -\frac{Re}{32A^{10}}\overline{\phi_\xi^-}(x)+\frac{B}{4A^4}\left\{\frac{[1+S\eta^2]^{\frac{1}{2}}}{\eta}\overline{u^-}(x)\right\}_x-\frac{B^{\frac{3}{2}}}{A}\left\{\frac{[1+S\eta^2]^{\frac{3}{4}}e^{\frac{1}{2}x}}{\eta^2}\overline{\psi^-}(x)\right\}_x. \tag{2.53}$$

Similarly, from (2.51) we may derive the relation

$$B^2\eta^{-4}[1+S\eta^2]\,\chi_y(x,y_T)-2AB^{\frac{3}{2}}\{\eta^{-2}[1+S\eta^2]^{\frac{3}{4}}\,e^{\frac{1}{2}x}\,\chi_x(x,y_T)\}_x$$
$$= g^+(x) = -\frac{Re}{32A^{10}}\bar{\phi}_x(x)+\frac{B}{4A^4}\left\{\frac{[1+S\eta^2]^{\frac{1}{2}}}{\eta}\bar{u}(x)\right\}_x+\frac{B^{\frac{3}{2}}}{A}\left\{\frac{[1+S\eta^2]^{\frac{3}{4}}e^{-x}}{\eta^2}\bar{\psi}(x)\right\}_x. \tag{2.54}$$

Equations (2.53) and (2.54) are the two boundary conditions that the master potential χ must satisfy at the ends of the cylinder. They relate linear combinations of the derivatives of χ to the functions $g^{\pm}(x)$, which in turn are determined by the prescribed boundary conditions on the flow variables at the ends of the cylinder. Note that by setting $\eta = 1$ wherever it appears algebraically in (2.50), (2.51), (2.53) and (2.54) yields the Carrier–Maslen conditions that hold when the effects of curvature are neglected (Wood & Morton 1980).

2.4. *Summary of the problem*

We have now completed the formulation of the problem for the master potential χ. First, in the region $D = \{x, y\colon 0 < x < x_T,\ 0 < y < y_T\}$, χ satisfies the differential equation (2.29). At $x = x_T$ and for $0 \leqslant y \leqslant y_T$, χ satisfies the boundary conditions (2.30), (2.31) and (2.33), while, at $x = 0$ and for $0 \leqslant y \leqslant y_T$, the boundary conditions are given by (2.34), (2.35) and (2.37). At $y = 0$ and for $0 \leqslant x \leqslant x_T$, χ satisfies the boundary condition (2.53), while, at $y = y_T$ and for $0 \leqslant x \leqslant x_T$, the boundary condition is given by (2.54).

In §3 we will discuss how to obtain finite-element approximations for the master potential χ. Once χ, or an approximation of χ, has been obtained, some variables of physical interest can be obtained by differentiation. In particular, from (2.23), (2.24) and (2.28) we have that the dimensionless perturbation stream function, radial velocity and axial velocity are given respectively by

$$\psi = -2A^2\chi_x, \quad u = 2A^2\chi_{xy} \quad \text{and} \quad w = 4A^4\chi_{xx} \tag{2.55), (2.56), (2.57}$$

To obtain the auxiliary variable ϕ, we would integrate (2.36) and (2.52). Of course, by (2.16), ϕ is merely a linear combination of the dimensionless perturbation temperature T and azimuthal velocity v. In order to recover T and v themselves, we must solve for another auxiliary variable H, which is defined by

$$H = T+2S\eta^2 v. \tag{2.58}$$

A differential equation for H is easily obtained from the linearized equations of motion, and is given by (Maslen 1979)

$$H_{yy}+4A^4\left\{(1+S\eta^2)\left(\frac{H}{1+S\eta^2}\right)_x\right\}_x = 0. \tag{2.59}$$

The boundary conditions that H must satisfy are also easily derived. They are given by

$$\left.\begin{aligned} H_x &= 0 \quad \text{at} \quad x = x_{\mathrm{T}}, \\ H &= \theta(y) \quad \text{at} \quad x = 0 \end{aligned}\right\} \quad \text{for} \quad 0 \leqslant y \leqslant y_{\mathrm{T}},$$

and

$$H = \bar{H}(x) = \bar{T}(x) + 2S\eta^2\bar{v}(x) \quad \text{for} \quad 0 \leqslant x \leqslant x_{\mathrm{T}},$$

at the top and bottom of the cylinder. Note that the problem for H is a second-order elliptic boundary-value problem.

We will not consider the H-problem any further in this work, as we are primarily interested in the stream function ψ. The reason for this is that the separative properties of the flow can be determined from ψ alone (Von Halle 1977; Hoglund *et al.* 1979). However, note that if one is interested in the thermal properties of the flow, then one must solve for H as well as χ. Finally, we note that the perturbation pressure p and density ρ may be obtained from (2.3), (2.5) and (2.7).

3. The Galerkin finite-element algorithm

We wish to reformulate our boundary-value problem for the master potential χ into a Galerkin formulation. This is accomplished by standard procedures (Strang & Fix 1972), which consist of the following steps:

(i) multiply (2.29) by a smooth function $\tilde{\chi}$ that satisfies the boundary conditions $\tilde{\chi} = \tilde{\chi}_x = 0$ at $x = x_{\mathrm{T}}$ and $\tilde{\chi}_x = \tilde{\chi}_{xx} = 0$ at $x = 0$;

(ii) integrate the result over the domain $D = \{x, y: 0 < x < x_{\mathrm{T}}, 0 < y < y_{\mathrm{T}}\}$;

(iii) integrate the term involving x-derivatives by parts three times and the term involving y-derivatives by parts once;

(iv) use the boundary conditions (2.30), (2.37), (2.53) and (2.54) for χ and the above conditions for $\tilde{\chi}$ to evaluate the resulting boundary integrals.

These steps yield

$$\begin{aligned} \iint_D \left\{\eta^2 \mathrm{L}_3\chi \mathrm{L}_3\tilde{\chi} + B^2\frac{1+S\eta^2}{\eta^4}\chi_y\tilde{\chi}_y\right\}\mathrm{d}x\,\mathrm{d}y \\ -2AB^{\frac{3}{2}}\int_0^{x_{\mathrm{T}}}\left\{\frac{(1+S\eta^2)^{\frac{3}{4}}}{\eta^2}\mathrm{e}^{\frac{1}{2}x}\chi_x\tilde{\chi}\right\}\Big|_{y=y_{\mathrm{T}}}\mathrm{d}x - 2AB^{\frac{3}{2}}\int_0^{x_{\mathrm{T}}}\left\{\frac{(1+S\eta^2)^{\frac{3}{4}}}{\eta^2}\mathrm{e}^{\frac{1}{2}x}\chi_x\tilde{\chi}\right\}\Big|_{y=0}\mathrm{d}x \\ -\int_0^{x_{\mathrm{T}}}\{g\tilde{\chi}|_{y=y_{\mathrm{T}}} - g\tilde{\chi}|_{y=0}\}\,\mathrm{d}x + \int_0^{y_{\mathrm{T}}}(f\tilde{\chi})|_{y=0}\,\mathrm{d}x = 0, \end{aligned} \tag{3.1}$$

where

$$\mathrm{L}_3\chi \equiv (\mathrm{e}^x\chi_{xx})_x. \tag{3.2}$$

The next steps are given by:

(i) integrate the second and third integrals in (3.1) by parts with respect to x;

(ii) use the boundary condition $\tilde{\chi} = 0$ at $x = x_{\mathrm{T}}$ and the boundary condition (2.35) for χ, evaluated at $y = 0$ and $y = y_{\mathrm{T}}$, in order to evaluate the resulting boundary integrals.

These steps result in

$$\mathrm{B}(\chi, \tilde{\chi}) = \mathrm{F}(\tilde{\chi}), \tag{3.3}$$

where

$$\mathrm{F}(\tilde{\chi}) \equiv -\int_0^{y_{\mathrm{T}}}(f\tilde{\chi})|_{x=0}\,\mathrm{d}y + \int_0^{x_{\mathrm{T}}}(g\tilde{\chi}|_{y=y_{\mathrm{T}}} - g\tilde{\chi}|_{y=0})\,\mathrm{d}x \tag{3.4}$$

and
$$B(\chi,\tilde{\chi}) \equiv \iint_D \left\{\eta^2 L_3\chi\, L_3\tilde{\chi} + B^2\frac{1+S\eta^2}{\eta^4}\chi_y\tilde{\chi}_y\right\}dx\,dy$$
$$+2AB^3_2\int_0^{x_T} e^{\frac{1}{2}x}\frac{(1+S\eta^2)^{\frac{3}{4}}}{\eta^2}\{(\chi_x\tilde{\chi}_x)|_{y=y_T}+(\chi_x\tilde{\chi}_x)|_{y=0}\}\,dx. \quad (3.5)$$

Our approximate solution is defined by first choosing a finite-dimensional finite-element space of functions, which we denote by S^h, and then seek a $\chi^h \in S^h$ such that

$$B(\chi^h,\tilde{\chi}^h) = F(\tilde{\chi}^h) \quad \text{for all} \quad \tilde{\chi}^h \in S^h. \quad (3.6)$$

The functions in the space S_h should satisfy the following requirements:

(i) they must be twice continuously differentiable with respect to x and once continuously differentiable with respect to y;

(ii) they must satisfy the boundary conditions (2.31) and (2.33)–(2.35).

These requirements are necessary in order for the integrals in (3.6) to be well-defined and for the approximate solution χ^h to satisfy the correct boundary conditions. Note that the remaining boundary conditions, namely (2.30), (2.37), (2.53) and (2.54), are automatically accurately, although not exactly, satisfied by any solution of (3.6).

The particular functions that we utilize are products of piecewise-cubic spline functions of x and piecewise-linear functions of y. For all details concerning the derivation, analysis and implementation of the finite-element algorithm see Eastham (1981), Gunzburger & Wood (1982), Gunzburger *et al.* (1984) and Jordan (1983). Here we merely point out that the associated matrix problem that results from the finite-element discretization is symmetric and positive-definite. These are true whether or not the effects of curvature are retained in the derivation of the model. Also we note that the approximate solutions for the master potential χ^h, the perturbation streamfunction ψ^h and the perturbation axial velocity w^h are all second-order accurate, where of course ψ^h and w^h are obtained from χ^h by differentiation, i.e. by (2.55) and (2.57). On the other hand, the approximation u^h to the perturbation radial velocity obtained through (2.56) is only first-order accurate (for details see Eastham 1981).

4. Comparisons of models with and without curvature effects

A computer code was developed to implement the algorithm of §3. The code was written in such a way that it can be used in conjunction with the pancake model or with the present model by making the choice

$$\eta(x) = \begin{cases} 1 & \text{for pancake model,} \\ \left[1-\dfrac{x}{A^2}\right]^{\frac{1}{2}} & \text{for model with curvature terms.} \end{cases} \quad (4.1)$$

Other than in the choice of this function, the code is identical for both models.

Here we present numerical results for two different methods of inducing a countercurrent flow in the centrifuge. In the first method, the perturbed flow is induced by a linear temperature distribution along the cylinder wall, with the temperature at the two ends of the cylinder being constant and equal to the corresponding value at the wall. The end-to-end temperature difference is 1 K, with the hotter end at the bottom. This case was studied by Wood & Morton (1980) and Gunzburger & Wood (1982). In the second method, the perturbed flow is induced by

Length L	335.3 cm
Radius a	9.145 cm
Wall pressure p_w	13.3 kPa
Ambient temperature T_0	300 K
Peripheral speed Ωa	400, 500, 700 m/s

TABLE 1. Centrifuge parameters

injecting and removing mass through the ends of the cylinder. A uniform axial mass flux of unit amplitude is introduced through the interval $7 \leqslant x \leqslant 8$ at the end $y = 0$ and the interval $1 \leqslant x \leqslant 2$ at the end $y = y_T$. A like amount of mass flux is removed through the interval $1 \leqslant x \leqslant 2$ at the end $y = 0$ and the interval $7 \leqslant x \leqslant 8$ at the end $y = y_T$. In this case isothermal boundaries are assumed. This type of countercurrent drive has been studied by Soubbaramayer (1979) and Gunzburger & Wood (1982).

The centrifuge parameters used in the calculations are described in table 1. These represent a hypothetical centrifuge which has been previously considered by May (1977), Durivault & Louvet (1976), Wood & Morton (1980), Gunzburger & Wood (1982) and Gunzburger *et al.* (1984).

In all calculations a non-uniform grid spacing was employed. The distribution of grid points was determined by the transformations $x = \bar{x}^2/x_T$ and $y = y_T \sin^2(\pi\bar{y}/2y_T)$, with a uniform spacing in the $\bar{x}$- and $\bar{y}$-coordinates. Calculations for the linear wall-temperature drives were performed using a 24×24 mesh, and it was found that the choice $x_T = 8$ was sufficiently large for any further increases in x_T to have a negligible effect on the numerical solution. The cases involving axial mass fluxes through the ends of the cylinder were performed using 35 radial and 20 axial grid points and with $x_T = 11$. For these cases a larger value of x_T was required owing to the introduction and removal of mass high in the 'atmosphere', i.e. through the interval $7 \leqslant x \leqslant 8$.

With the choice of parameters given above, the inhomogeneities of the mathematical problem for the master potential χ are given by

$$g^+(x) = g^-(x) = 0, \quad f(y) = -\frac{Re}{32A^{10}T_0 y_T}$$

for the linear wall-temperature-drive case. For the mass-throughput cases we have that $f(y) = 0$ and $g^+(x)$ and $g^-(x)$ are determined from their definition in (2.53) and (2.54) respectively, with the choices $u^{\pm}(x) = 0$, $\phi^{\pm}(x) = 0$ and

$$\overline{\psi^{\pm}}(x) = -\frac{1}{2A^2} \times \begin{cases} 0 & \text{for } x \leqslant 1 \text{ and } x \geqslant 8, \\ x-1 & \text{for } 1 \leqslant x \leqslant 2, \\ 1 & \text{for } 2 \leqslant x \leqslant 7, \\ 8-x & \text{for } 7 \leqslant x \leqslant 8. \end{cases}$$

The parameters A, B, Re and S are easily determined from their definitions, the centrifuge parameters of table 1 and choices for R, k and μ corresponding to a particular gas. In our calculations the gas is chosen to be uranium hexafluoride.

Figures 1–5 contain comparisons of the numerical solutions obtained with and without retaining curvature terms in the model, i.e. comparisons of results obtained using the two choices for $\eta(x)$ contained in (4.1). Each figure corresponds to one of the two methods of inducing a countercurrent flow and to a particular choice for the peripheral speed Ωa. Three types of comparisons are provided in each figure. In parts

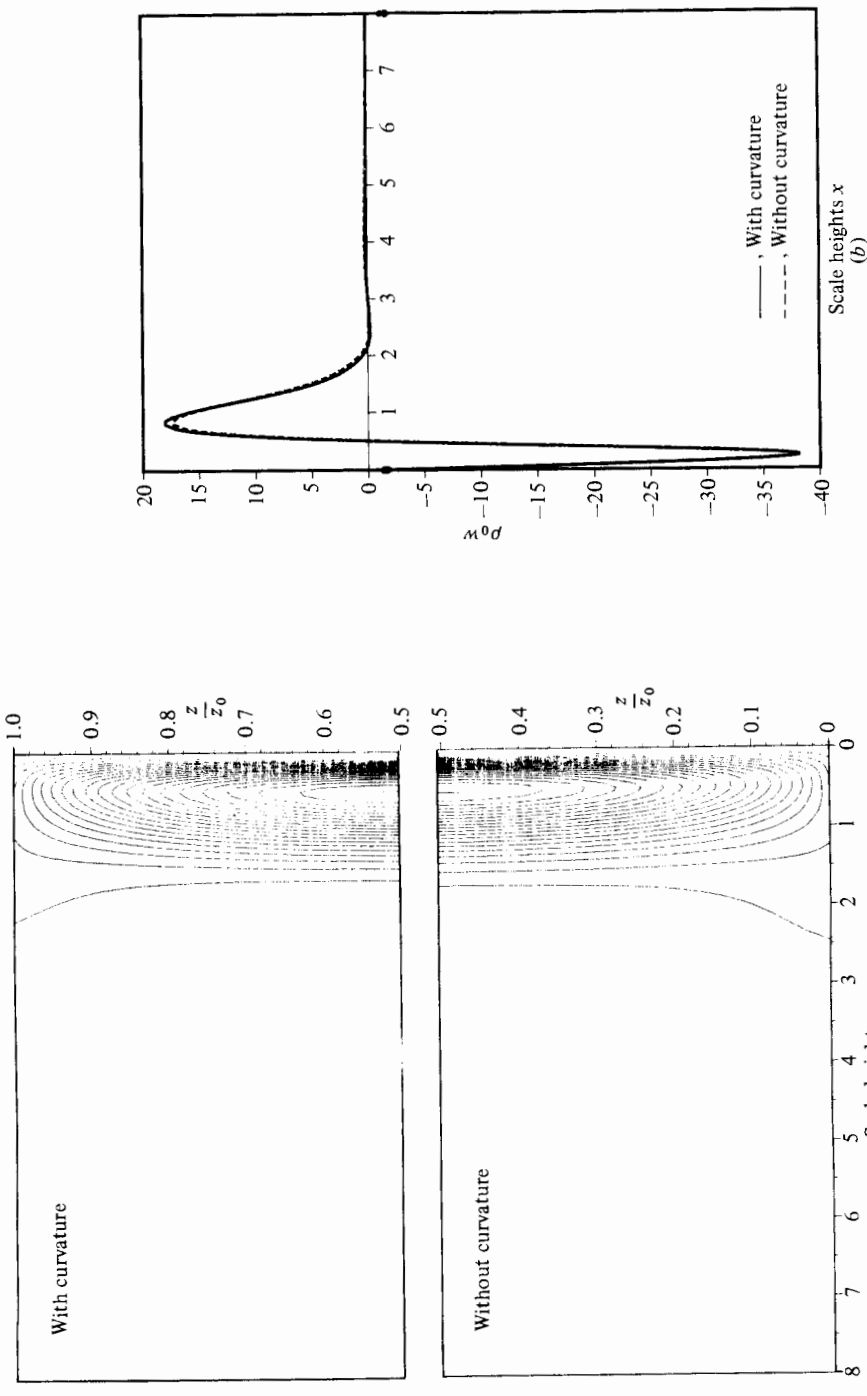

FIGURE 1. For caption see facing page.

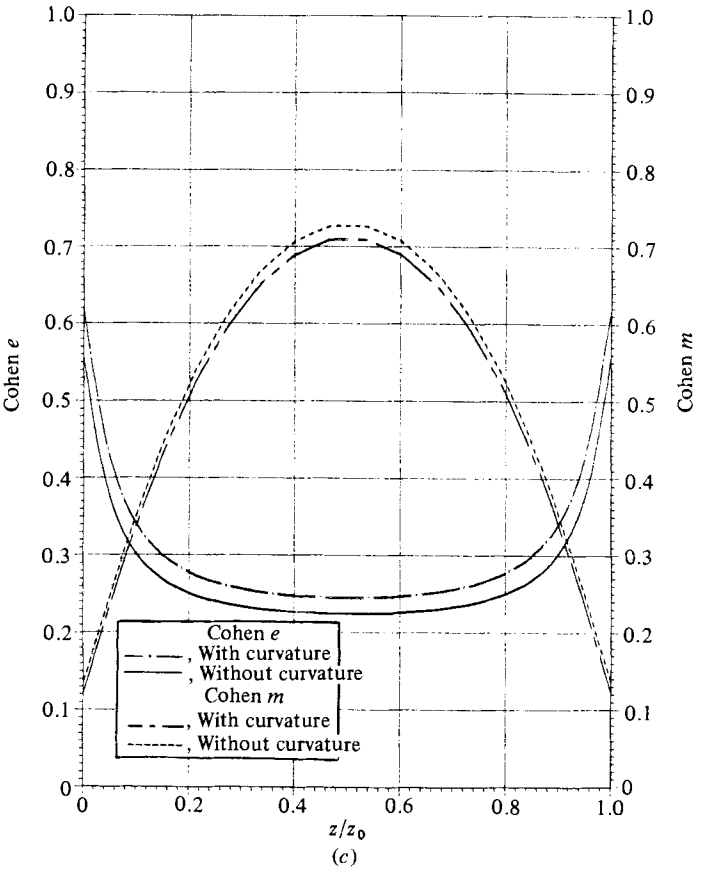

FIGURE 1. (*a*) Streamlines for linear wall-temperature drive at 400 m/s. (*b*) Axial mass flux versus radial position at $y = \frac{1}{4}y_T$ for linear wall-temperature drive at 400 m/s. (*c*) Cohen's e and m versus axial position for linear wall-temperature drive at 400 m/s.

(*a*) of the figures we compare the level lines of the stream function $\psi(x, y)$. The stream function is symmetric about the midplane $y = \frac{1}{2}$ for all our cases; therefore we show only the flow region $y \geqslant \frac{1}{2}$ for results obtained including curvature terms, and the flow region $y \leqslant \frac{1}{2}$ for the corresponding case in which η has been set to unity. The second comparisons are provided in parts (*b*), wherein profiles of the axial mass flux $\rho_0 w = \exp(-x)\, w(x, y)$, given in units of g m^{-2} s^{-1} at a fixed axial position ($y = \frac{1}{4}y_T$) are given. The final pictorial comparisons, contained in part (*c*), are of $e_F(y)$ and $m(y)$. The former, commonly referred to as 'Cohen's e', is the flow-pattern efficiency and depends solely on the shape of the axial-velocity profile of the circulating gas. The latter, commonly referred to as 'Cohen's m' is a variable which is directly proportional to the upflow rate. Both quantities are determined from integrals of the axial mass flux. For the precise definitions of e_F and m, and for a detailed discussion of the role they play in determining the separative performance and the design of centrifuges, see Soubbaramayer (1979), or Hoglund *et al.* (1979). Here we content ourselves by noting that it is desirable to have e_F as large as possible and for m to have an optimal shape which will depend on the methods of introducing and withdrawing gas.

Tables 2–4 provide a quantitative comparison of the numerical solutions obtained with and without retaining curvature terms. We let $\psi_c(x, y)$ and $\psi_0(x, y)$ denote respectively the stream functions of the flow fields obtained with and without the

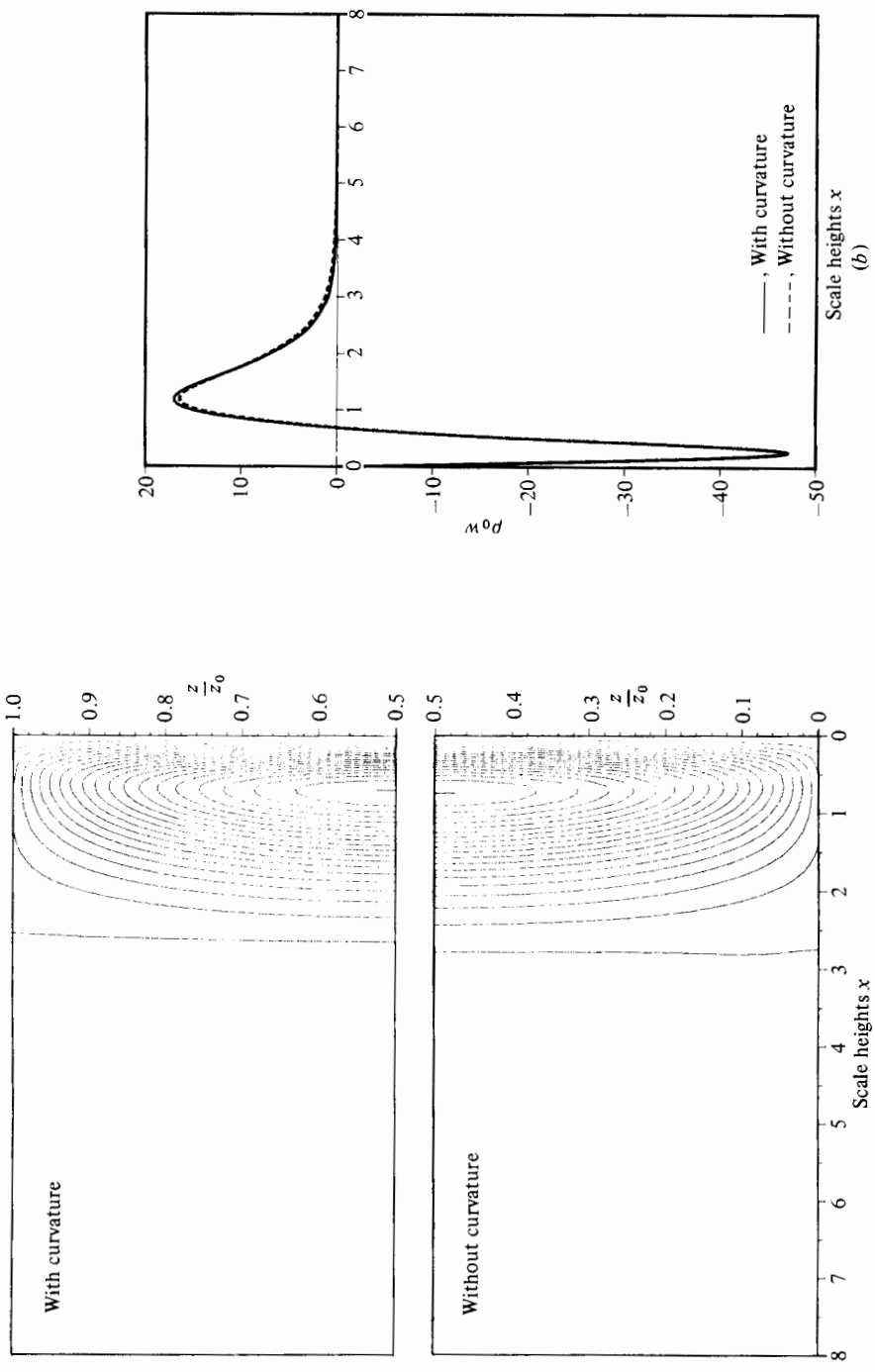

FIGURE 2. For caption see facing page.

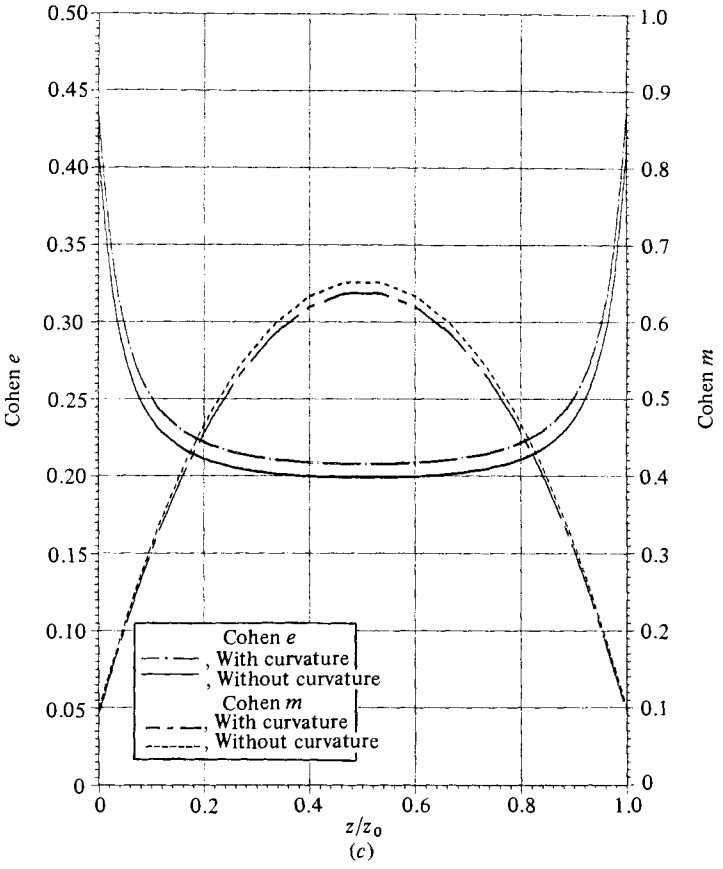

FIGURE 2. (*a*) Streamlines for linear wall-temperature drive at 500 m/s. (*b*) Axial mass flux versus radial position at $y = \frac{1}{4}y_T$ for linear wall-temperature drive at 500 m/s. (*c*) Cohen's e and m versus axial position for linear wall-temperature drive at 500 m/s.

inclusion of the effects of curvature. In table 2 we tabulate, for different values of the peripheral speed, the normalized root-mean-square difference

$$d = \left[\frac{\int_0^{y_T} \int_0^{x_T} (\psi_c - \psi_0)^2 \, dx \, dy}{\int_0^{y_T} \int_0^{x_T} \psi_c^2 \, dx \, dy} \right]^{\frac{1}{2}}.$$

To get a better idea of how the difference between ψ_c and ψ_0 are distributed around the flow field, in table 3 we give, for selected values of the peripheral speed, the following normalized root-mean-square differences:

$$\delta_1(x) = \frac{1}{d}\left[\int_0^{y_T} (\psi_c - \psi_0)^2 \, dy \right]^{\frac{1}{2}}$$

and

$$\delta_2(x) = \left[\frac{\int_0^{y_T} (\psi_c - \psi_0)^2 \, dy}{\int_0^{y_T} \psi_c^2 \, dy} \right]^{\frac{1}{2}}.$$

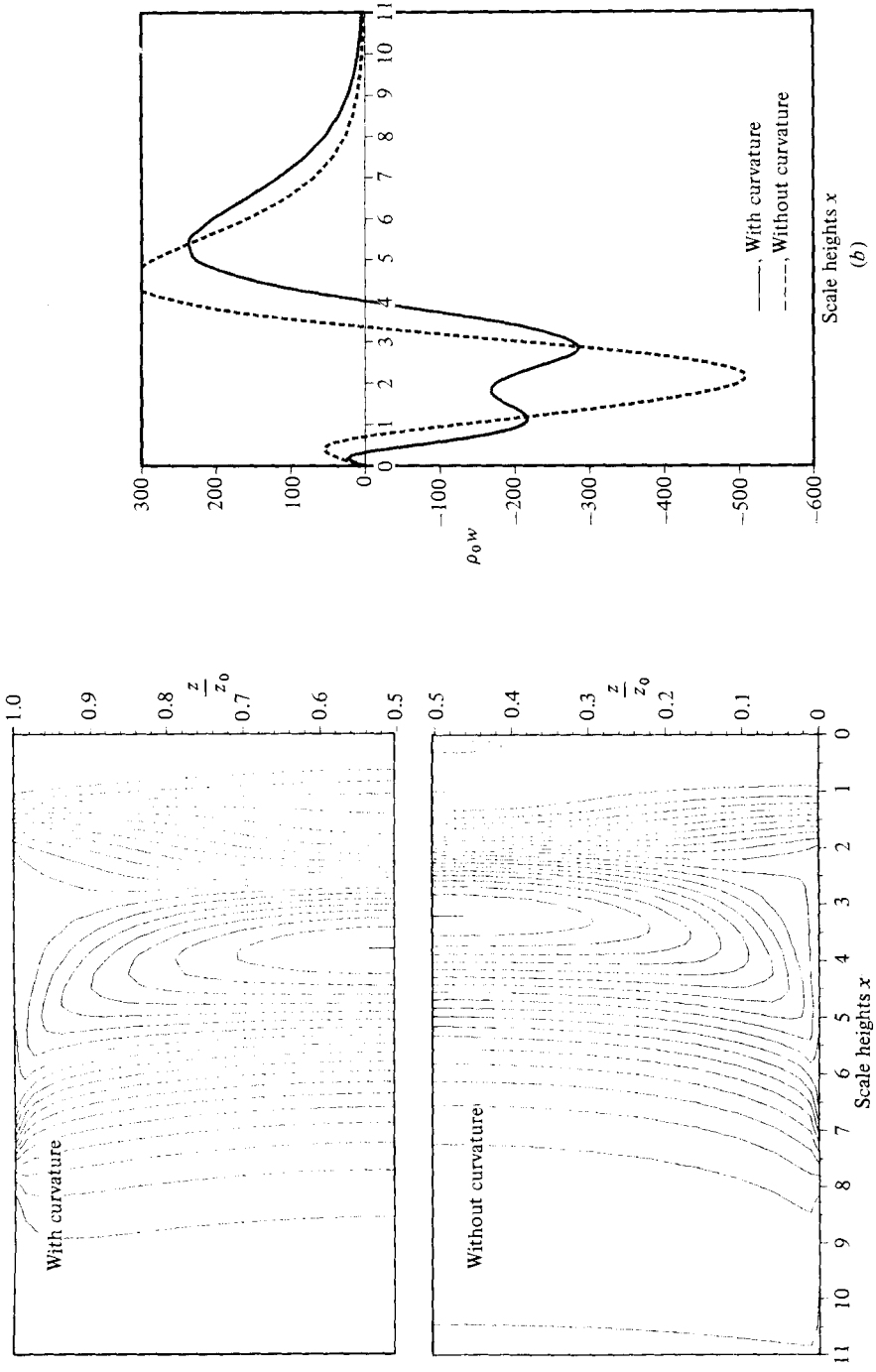

FIGURE 3. For caption see facing page.

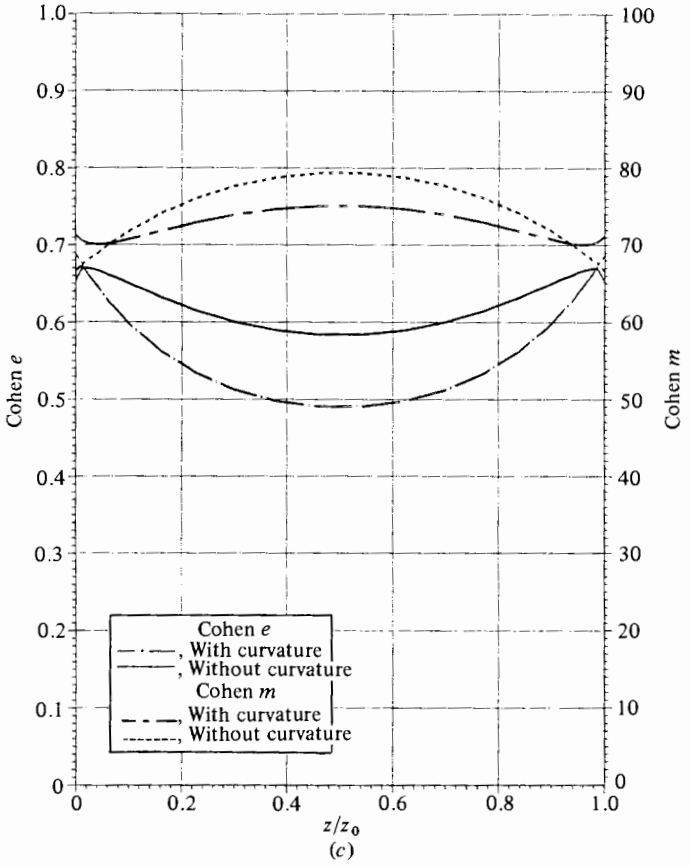

FIGURE 3. (*a*) Streamlines for mass-throughput drive at 400 m/s. (*b*) Axial mass flux versus radial position at $y = \frac{1}{4}y_T$ for mass-throughput drive at 400 m/s. (*c*) Cohen's e and m versus axial position for mass-throughput drive at 400 m/s.

These provide information about how the difference between ψ_c and ψ_0 are distributed radially in the centrifuge. Note that, owing to the different normalization, $\delta_1(x)$ measures a local difference relative to the global difference d, while $\delta_2(x)$ measures a local difference relative to the size of the stream function at the same local position.

Table 4 provides similar information for the axial distribution of the differences between ψ_c and ψ_0, i.e.

$$\epsilon_1(y) = \frac{1}{d}\left[\int_0^{x_T} (\psi_c - \psi_0)^2 \, dx\right]^{\frac{1}{2}}$$

and

$$\epsilon_2(y) = \left[\frac{\int_0^{y_T} (\psi_c - \psi_0)^2 \, dx}{\int_0^{y_T} \psi_c^2 \, dx}\right]^{\frac{1}{2}}.$$

4.1. *Discussion of numerical results*

An examination of the pictorial and tabular results first reveals the obvious. As the rotational speed Ωa increases, the effects of curvature decrease. In fact, we have not provided any figures for the case of a linear wall-temperature drive with a peripheral

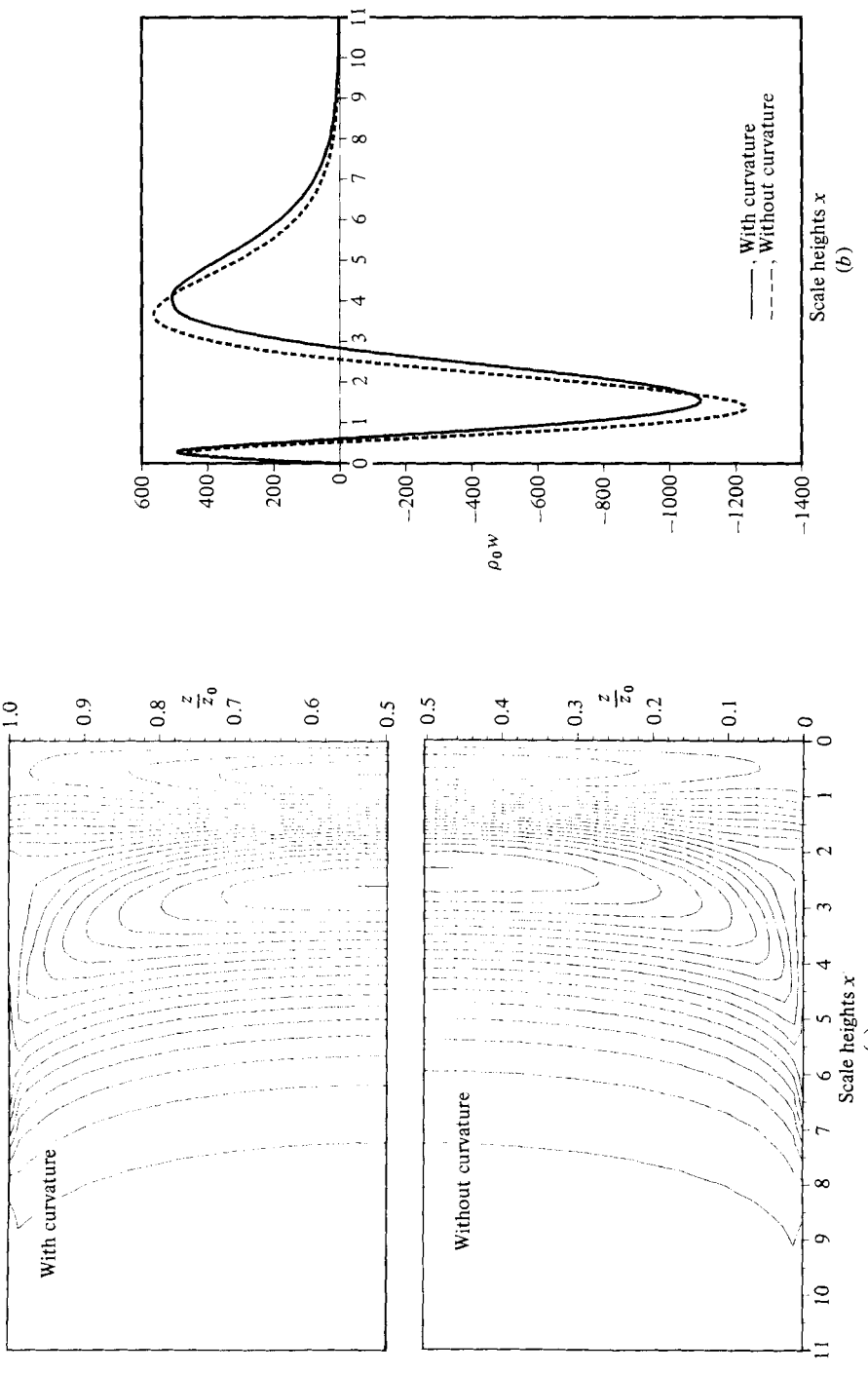

FIGURE 4. For caption see facing page.

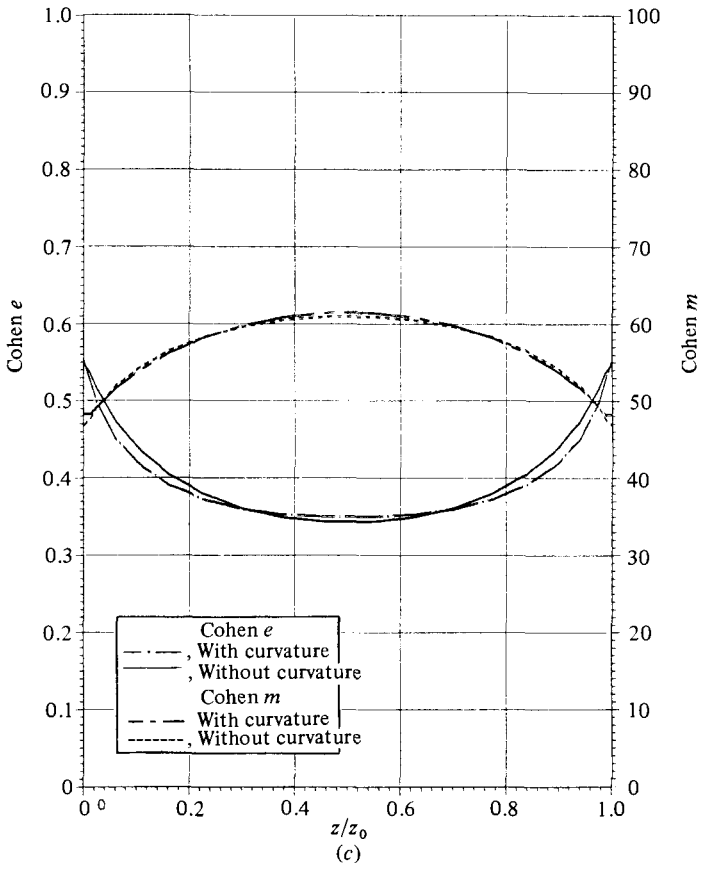

FIGURE 4. (*a*) Streamlines for mass-throughput drive at 500 m/s. (*b*) Axial mass flux versus radial position at $y = \frac{1}{4}y_T$ for mass-throughput drive at 500 m/s. (*c*) Cohen's *e* and *m* versus axial position for mass-throughput drive at 500 m/s.

speed of 700 m/s, because in this case the pictorial representation of the solutions obtained with and without the inelusion of the terms due to curvature are essentially indistinguishable.

A second fact that is also immediately evident from the numerical results is that the effects of curvature are much more pronounced for the flow induced by the introduction and removal of mass through the ends of the centrifuge than for the flow induced by a temperature gradient along the cylindrical wall of the centrifuge. This is most probably due to the fact that, in the former case, we are introducing and removing mass through openings located between 7 and 8 scale heights so that a more significant portion of the total mass of fluid in the centrifuge is found in regions away from the wall. This is clear from the streamline and axial-mass-flux plots. Note especially the substantial differences in the solutions obtained with and without curvature terms for the mass throughput case with $\Omega a = 400$ m/s.

For example, one of the more prominent differences is illustrated by the axial-mass-flux profiles with and without curvature for the mass throughput case with $\Omega a = 400$ m/s shown in figure 3(*b*). This figure shows the profiles at $y = \frac{1}{4}y_0$, one quarter of the rotor length measured from the bottom. Similar plots of calculated profiles closer to the bottom reveal that, just outside the Ekman layer, the with and without curvature profiles are the same except for a radial shifting and the extra hump

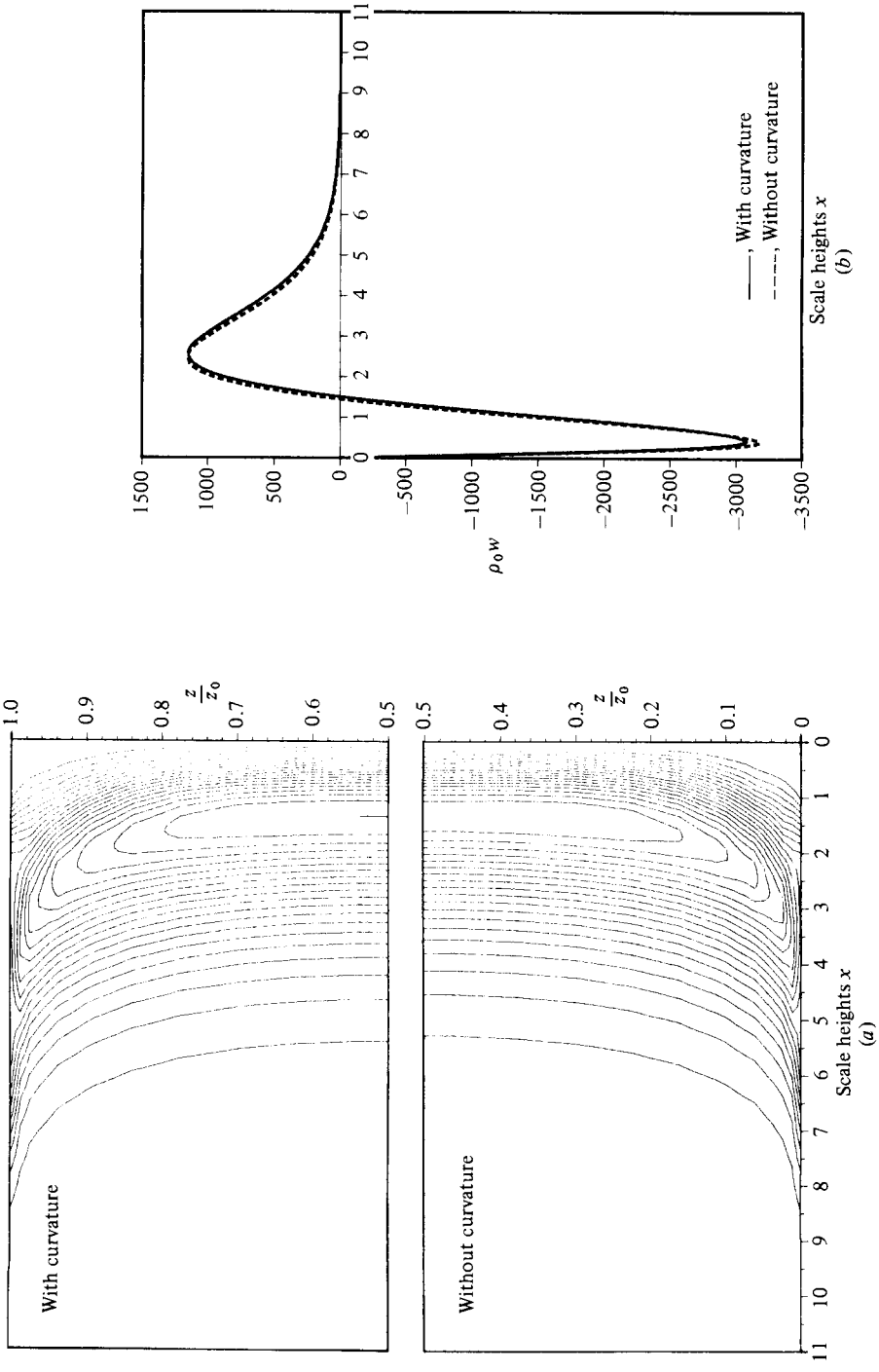

FIGURE 5. For caption see facing page.

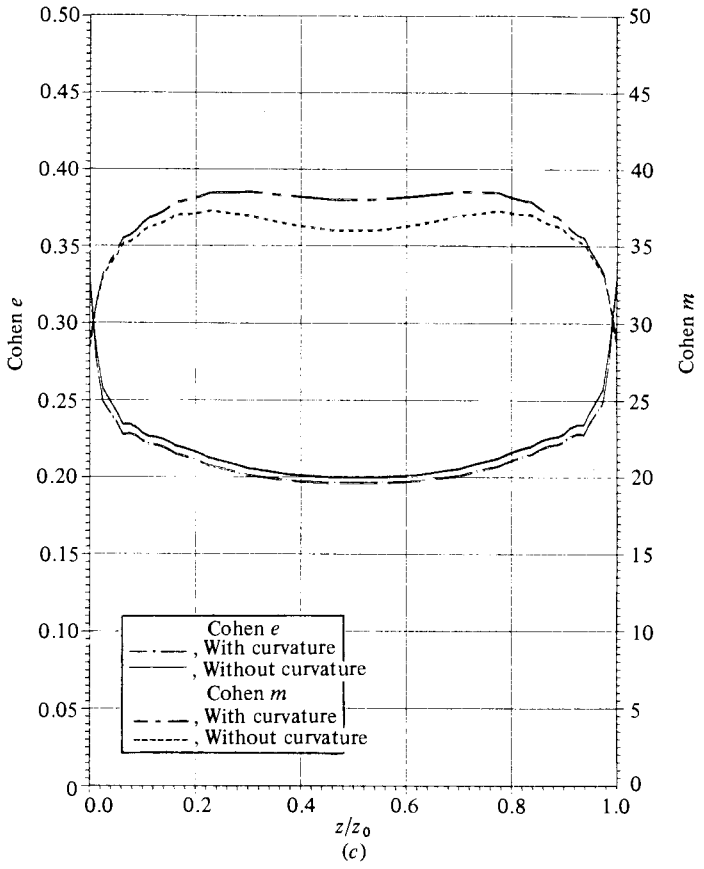

FIGURE 5. (*a*) Streamlines for mass-throughput drive at 700 m/s. (*b*) Axial mass flux versus radial position at $y = \frac{1}{4}y_T$ for mass-throughput drive at 700 m/s. (*c*) Cohen's *e* and *m* versus axial position for mass-throughput drive at 700 m/s.

Peripheral speed Ωa	*d* for LWT	*d* for MT
400 m/s	0.051	0.301
500 m/s	0.039	0.173
700 m/s	0.013	0.055

TABLE 2. Normalized root-mean-square difference in the stream function computed with and without the inclusion of curvature terms; LWT = linear wall-temperature drive, MT = mass-throughput drive

shown in figure 3(*b*) is present in both curves but is further from the rotor wall at about 7 scale heights. As the distance from the end of the rotor increases, the hump moves toward the rotor wall in both cases, but the amplitude decreases more rapidly in the without-curvature case until it has disappeared at $\frac{1}{4}y_0$. At the peripheral speed of 400 m/s, the hump in the with-curvature case persists throughout the rotor. Calculations performed for higher peripheral speeds of 500 and 700 m/s reveal the same feature except the hump has decayed from both profiles within the first 10% of the rotor length. This behaviour has also been observed in similar mass-throughput calculations based on finite-difference solutions.

	LWT (Ωa = 400 m/s)		MT (Ωa = 40 m/s)		MT (Ωa = 700 m/s)	
x	δ_1	δ_2	δ_1	δ_2	δ_1	δ_2
1	0.0388	0.059	0.084	1.250	0.0228	0.0392
2	0.0210	0.442	0.087	0.325	0.0295	0.0447
3	0.0149	0.332	0.210	0.448	0.0324	0.0729
4	0.0125	0.398	0.050	0.084	0.0215	0.1019
5	0.0065	0.407	0.110	0.228	0.0105	0.0867
6	0.0027	0.405	0.104	0.354	0.0057	0.0622
7	0.0012	0.547	0.062	0.392	0.0036	0.0715
8	—	—	0.028	0.505	0.0008	0.0449
9	—	—	0.011	0.546	0.0003	0.0560
10	—	—	0.003	0.567	0.0001	0.0855

TABLE 3. Radial distribution of the differences between ψ_c and ψ_0; Ωa = peripheral speed, LWT = linear wall-temperature drive, MT = mass-throughput drive

	LWT (Ωa = 400 m/s)		MT (Ωa = 400 m/s)		MT (Ωa = 700 m/s)	
y	ϵ_1	ϵ_2	ϵ_1	ϵ_2	ϵ_1	ϵ_2
0	0.0300	0.1358	0.0525	0.0559	0.0178	0.0235
$\frac{1}{4}$	0.0518	0.0507	0.3121	0.3102	0.0537	0.0517
$\frac{1}{2}$	0.0608	0.0470	0.3895	0.3754	0.0594	0.0578

TABLE 4. Axial distribution of the differences between ψ_c and ψ_0; Ωa = peripheral speed, LWT = linear wall-temperature drive, MT = mass-throughput drive

Insofar as the radial and axial distributions of the stream functions are concerned, not many general trends seem to be evident from the figures on tables 3 and 4 and from other calculations. For example, for the linear wall-temperature drive, $\epsilon_2(y)$ seems to be largest near the centre of the centrifuge (i.e. $y = \frac{1}{2}$), while for the mass-throughput drive it is largest near the ends. On the other hand, $\epsilon_1(y)$ seems to be consistently larger near the centre of the centrifuge. This is probably due to the fact that the total mass flow through planes y = constant is greatest for $y = \frac{1}{2}$. The results for $\delta_1(x)$ and $\delta_2(x)$ are even less consistent; however, it is clear that they depend heavily on the number of cells in the flow. For example, compare the double peak in the distribution of $\delta_1(x)$ for the case MT (Ωa = 400 m/s) with the results for the other cases of table 3. Then note the multicelled flow of figure 3 (a) and the single-celled flows of figures 1 (a) and 5 (a).

5. Conclusions

The results obtained indicate that the inclusion of terms that account for the effects of curvature in the model equations governing the flow in rapidly rotating centrifuges can have a significant effect on the resulting solutions. This is especially true at relatively low rotational speeds and for other cases where large amounts of mass are found in flow regions away from the wall of the centrifuge. Of course, the particular gas being considered determines the stratifications, so that these effects could also be studied at a fixed rotational speed for gases of various molecular weights.

The finite-element technique, used to obtain approximate solutions of the

governing equations, is as easily implemented when curvature terms are retained as when they are not. Also, the accuracy of the numerical solution is not significantly affected. Therefore use of the finite-element technique to determine the flow field in the centrifuge enables one to discard, without penalty, the 'pancake' assumption in the Onsager model. Still to be determined are the effects of curvature on flows driven by sources or sinks of mass, momentum and energy and subsequently, the effects of curvature on the separative performance of gas centrifuges. Again, it seems that the use of finite-element techniques will make such studies easily accessible.

This work, as any dealing with flows in gas centrifuges, owes a great deal to the work of George Carrier, Stephen Maslen and, of course, to the late Lars Onsager. The authors also wish to express their appreciation to Edward Von Halle for his many insightful comments.

This work was supported by the U.S. Department of Energy under Contract DE-AC05-82OR20900.

REFERENCES

BABARSKY, R. & WOOD, H. G. 1982 An analysis from first principles of the source/sink terms in the pancake equation. *Univ. Virginia, Charlottesville, Rep.* UVA-ER-795-82.

DURIVAULT, J. & LOUVET, P. 1976 Etude théorique de l'écoulement dans une centrifugeuse – contre-courant thermique. *Centre d'Etudes Nucléaires de Saclay, Rep. CEA*-R-4714.

EASTHAM, J. F. 1981 The finite element method in anisotropic Sobolev spaces. Ph.D. thesis, University of Tennessee, Knoxville, Tennessee.

GUNZBURGER, M. D. & WOOD, H. G. 1982 A finite element method for the Onsager pancake equation. *Comp. Meth. Appl. Mech. Engng* **31**, 43–59.

GUNZBURGER, M. D., WOOD, H. G. & JORDAN, J. A. 1984 A finite element method for gas centrifuge problems. *SIAM J. Sci. Stat. Comp.* **5**.

HOGLUND, R. L., SHACTER, J. & VON HALLE, E. 1979 Diffusion separation methods. In *Encyclopedia of Chemical Technology* vol. 7, 3rd edn (ed. R. E. Kirk and D. F. Othmer). Wiley.

JORDAN, J. A. 1983 A numerical study of the effects of curvature on the fluid dynamics of gas centrifuges. M.S. thesis, University of Tennessee, Knoxville.

JUNG, E. 1983 An analytic solution of the linearized flow equations using the method of eigenvalues. In *Proc. of the 5th Workshop on Gases in Strong Rotation* (ed. H. G. Wood). University of Virginia, Charlottesville.

MASLEN, S. H. 1979 The basic steady-state flow models for computing countercurrent motions. *Univ. Virginia, Charlottesville, Rep.* UVA-ER-540-80.

MAY, W. G. 1977 *Separation Parameters of Gas Centrifuges. AIChE Symp. Series*, no. 169, vol. 73.

SOUBBARAMAYER, 1979 Centrifugation. In *Uranium Enrichment* (ed. S. Villani). Springer.

STRANG, G. & FIX, G. 1972 *An Analysis of the Finite Element Method.* Prentice-Hall.

VIECELLI, J. A. 1983 Exponential difference operator approximation for the sixth order Onsager equation. *J. Comp. Phys.* **50**, 162–170.

VON HALLE, E. 1977 The countercurrent gas centrifuge for the enrichment of U-235. In *Proc. 70th Ann. Meeting AIChE, New York.*

WOOD, H. G. & MORTON, J. B. 1980 Onsager's pancake approximation for the fluid dynamics of a gas centrifuge. *J. Fluid Mech.* **101**, 1–31.